NASA TECHNICAL MEMORANDUM

NASA TM X-71826

NASA TM X-71826

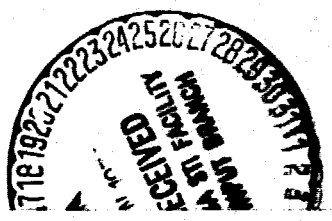

MEASUREMENT OF EXHAUST EMISSIONS FROM TWO J-58 ENGINES AT SIMULATED SUPERSONIC CRUISE FLIGHT CONDITIONS

by James D. Holdeman
Lewis Research Center
Cleveland, Ohio 44135

TECHNICAL PAPER to be presented at the 21st International Gas Turbine Conference sponsored by the American Society of Mechanical Engineers
New Orleans, Louisiana, March 21-25, 1976

MEASUREMENT OF EXHAUST EMISSIONS FROM TWO J-58 ENGINES AT SIMULATED SUPERSONIC CRUISE FLIGHT CONDITIONS

James D. Holdeman[1]

National Aeronautics and Space Administration
Lewis Research Center
Cleveland, Ohio 44135

E-8490

ABSTRACT

Emissions of total oxides of nitrogen, unburned hydrocarbons, carbon monoxide, and carbon dioxide from two J-58 afterburning turbojet engines at simulated high-altitude flight conditions are reported. Test conditions included flight speeds from Mach 2 to 3 at altitudes from 16 to 23 km. For each flight conditions, exhaust measurements were made for four or five power levels from maximum power without afterburning through maximum afterburning. The data show that exhaust emissions vary with flight speed, altitude, power level, and radial position across the exhaust. Oxides of nitrogen (NO_x) emissions decreased with increasing altitude, and increased with increasing flight speed. NO_x emission indices with afterburning were less than half the value without afterburning. Carbon monoxide and hydrocarbon emissions increased with increasing altitude, and decreased with increasing flight speed. Emissions of these species were substantially higher with afterburning than without.

INTRODUCTION

Testing of two J-58 afterburning turbojet engines was conducted in an altitude facility to determine their emissions of oxides of nitrogen,

---

[1]Aerospace Engineer, Combustion and Pollution Research Branch; Assoc. Mem. ASME

unburned hydrocarbons, carbon monoxide, and carbon dioxide at simulated supersonic, high-altitude flight conditions.

Emission measurements from aircraft turbine engines, and in particular afterburning engines at high-altitude supersonic flight conditions, are relevant to answering questions about the potential environmental impact of supersonic transports (SST's). Previous studies dealing with aircraft jet engine emissions at altitude conditions are reported in [1 to 6][2]. In these, various engines and flight conditions have been examined. The J-93 tests, [5], conducted at the Arnold Engineering and Development Center (AEDC) as part of the Climatic Impact Assessment Program, are the most closely related to the present investigation in terms of the size of the engine tested and flight conditions examined.

The purpose of the present investigation was to provide an emissions calibration for the J-58 engines for subsequent use in the NASA Stratospheric Jet Wake Experiment, (discussed in [7]). In this program, in-flight sampling of exhaust constituents will be made in the wake of a YF-12 aircraft, powered by two J-58 engines, during supersonic, stratospheric flight. The emissions calibration tests will provide the initial conditions for assessing the dispersion and dilution of exhaust products in the stratosphere and for evaluating jet/wake dispersion models such as that given in [8]. In addition, these tests will add to the general knowledge about emissions from afterburning turbojet engines at high altitude conditions. Although emission levels for the J-58 engine may not necessarily be representative of emissions from engines designed for present or future

[2]Numbers in brackets designate References at end of paper.

commercial supersonic aircraft, the trends should be similar.

The present investigation was conducted in the Propulsion Systems Laboratory at the NASA-Lewis Research Center. Some of the data from the first engine tested (herein designated as engine A), at Mach 2.0, 2.4, and 2.8 at 19.8 km, have been reported previously, [9 and 10]. Test conditions for the second engine (engine B) were Mach 2.0 at 16.0, 17.9, and 19.8 km; Mach 2.4 at 19.8 km; Mach 2.8 at 19.8, 22.0, and 23.5 km; and Mach 3.0 at 19.8 km. At each flight condition, data traverses across the horizontal diameter of the exhaust were made for four or five engine power levels from maximum power without afterburning through maximum afterburning. Results from tests on both engines are reported here. The engine A results are included both for completeness, and for comparison with the results of tests on engine B.

APPARATUS

The J-58 engine is an afterburning turbojet designed for operation at flight speeds in excess of Mach 2 at stratospheric altitudes. The two J-58 engines tested in this program will be installed in the NASA/USAF YF-12 aircraft for the flight tests in the NASA Stratospheric Jet Wake Experiment.

The engines were tested in the Propulsion Systems Laboratory at the NASA-Lewis Research Center. This altitude chamber facility and associated air handling equipment provided conditioned inlet airflow, and appropriate exhaust pressure to accurately simulate the conditions at the engine inlet and exhaust corresponding to the selected supersonic flight conditions. All tests were run using JP-7 fuel, which was heated to 395K prior to entering

the engine to simulate the condition on board the aircraft during supersonic flight. The atomic hydrogen-carbon ratio of this fuel is 2.0.

Emission measurements were made 7 cm downstream of the engine primary exhaust nozzle using a single point, traversing, water-cooled gas sample probe. The probe and its traversing mechanism are shown mounted behind the engine in Figure 1a. The traversing mechanism had the capability to translate the probe $\pm$60 cm horizontally and $\pm$20 cm vertically from the engine centerline.

The sensor area of the probe is shown in Figure 1b. A total pressure sensor was mounted 2.5 cm above the sample probe, and three unshielded iridium/iridium-rhodium thermocouples were mounted 2.5 and 5 cm below and 5 cm above the gas sample probe. The gas sample sensor had an i.d. of 0.717 cm. The probe tip extended 1.9 cm forward of the rake body. This section was water-cooled for a distance of 8 cm downstream from the tip, both for sample conditioning and probe integrity. Following this section, the sample line increased to 0.818 cm i.d. For afterburning conditions, a second water-cooled heat exchanger on the next 30 cm of line was used to provide additional quenching of the sample. Approximately 10 meters of 0.95 cm stainless-steel line was used to transport the sample to the analyzers. In order to prevent condensation of water, and to minimize adsorption-desorption effects of hydrocarbon compounds, the line was heated with steam at 428 K. Four heated metal bellows pumps (two pumps in series in each of two parallel legs) were used to supply sufficient gas sample pressure, 17 N/cm^2, to operate the analytical instruments. The gas sample line residence time was less than 2 seconds for

all test conditions.

The exhaust gas analysis system consists of four commercially available instruments, along with associated peripheral equipment necessary for sample conditioning and instrument calibration. In addition to the visual readout at the console, electrical inputs are provided to the facility computer for on-line analysis and data evaluation.

The hydrocarbon (HC) content of the exhaust gas was measured on a wet basis, using a Beckman Instruments Model 402 Hydrocarbon Analyzer. The instrument is of the flame ionization detector type. Both carbon monoxide (CO) and carbon dioxide (CO_2) were measured dry, using analyzers of the nondispersive infrared (NDIR) type. These instruments were Beckman instruments Model 315B. The concentration of the oxides of nitrogen (NO_x) was measured on a dry basis, using a Thermo Electron Corporation Model 10A Chemiluminescence Analyzer. This instrument includes a thermal converter to reduce nitrogen dioxide (NO_2) to nitric oxide (NO). Data were obtained as total NO_x ($NO + NO_2$).

TEST CONDITIONS AND PROCEDURE

The flight conditions simulated in the tests conducted on the J-58 engines are given in Table I. Test conditions 3, 4, 5 and 8 give variation of flight speed at an altitude of 19.8 km. This altitude would be a typical cruise altitude for advanced or second generation SST aircraft, and is the nominal altitude selected for the YF-12 flight experiments. For these conditions, combustor inlet temperature and pressure, and afterburner inlet pressure increase with increasing flight speed.

Conditions 1, 2 and 3 give variation of altitude at a constant flight speed of Mach 2.0. For these conditions, the combustor inlet temperature is constant. Combustor inlet pressure and afterburner pressure decrease with increasing altitude. Conditions 5, 6 and 7 also give altitude variation at constant flight speed, in these cases for Mach 2.8.

For each condition, the engine inlet air was conditioned to correspond in both temperature and pressure to the values at the engine face during flight. Also for each condition, tests were made at four or five engine power levels, including military power (maximum power without afterburning), minimum afterburning, maximum afterburning, and either one or two intermediate afterburning power levels. The altitude chamber pressure for each flight condition was selected to ensure that the flow was sonic at the engine primary exhaust nozzle. Note that the altitude chamber pressure does not need to be equal to the ambient static pressure for the simulated altitude, since the internal performance of the engine is correctly simulated for all external static pressures low enough to choke the nozzle. When installed on the aircraft, the engine exhaust passes through a secondary ejector nozzle, and leaves the tailpipe at supersonic velocity.

All eight flight conditions shown in Table 1 were tested for engine B. Engine A was tested at conditions 3, 4, and 5 only. Emission traverses were made at the plane of the primary nozzle (actually, the probe was 6.7 cm from the exit plane when the engine was cold with the nozzle wide open). Data were obtained at 5 cm (nominal) intervals across the horizontal exhaust diameter, resulting in approximately 20 data points per traverse. These small increments were necessary to document the steep gradients in

emissions and temperature found in afterburning operation. The interval was increased to nominally 7.5 cm for military power tests, since emissions and temperature gradients at this condition were much less than for afterburning conditions. The time required for each traverse varied from 30 to 45 minutes. Complete surveys, four or five power levels at each flight condition, required four to five hours of continuous engine operation.

At the Mach 2.0 condition for engine A, limited data were obtained up to 20 cm above and below the engine centerline on the vertical diameter. These data showed variations similar to chose on the horizontal diameter.

All gas analysis instruments were checked for zero and span prior to each traverse. Because the console allows rapid selection of zero, span, or sample modes, these frequent checks could be made during power level changes while the engine was running.

Concentrations which were measured on a dry basis (NO_x, CO, and CO_2) are reported on a wet basis, correcting for water vapor, including both inlet air humidity and water vapor from combustion [11]. The NO_x data have been corrected to zero ambient humidity conditions by multiplying the measured (wet basis) concentrations by EXP (19H), where H is the humidity of the engine inlet air expressed in g H_2O/g dry air [12]. The magnitude of this correction varied from 5 to 15 percent.

The local concentration data were mass weighted, and area integrated to obtain average concentrations. In this procedure, the exhaust was assumed to be sonic at the average total pressure, and the static pressure was calculated. The static pressure was assumed to be constant across

the exhaust. The exhaust nozzle radius, R_8, was calculated from the measured engine airflow, and average exhaust temperature and pressure. Average concentrations were obtained from the local measurements of total temperature, total pressure, and species concentration using a trapezoidal integration.

For each power level at each test condition, the measured concentrations of CO, CO_2, and HC were used to compute an emissions based fuel-air ratio using the relations given in reference 11. Although these calculated fuel-air ratios were within $\pm$15 percent of the metered fuel-air ratios (as specified in [11]), the gas sample fuel-air ratios were consistantly slightly higher than the metered values for the engine B tests, and the gas sample fuel-air ratios were consistently slightly less than the metered values for the engine A tests.

Emission indices, g pollutant/kg fuel, were calculated from the average concentration of each constituent, using both the gas sample and metered fuel air ratios. The ratio of these emission indices is approximately inversely proportional to the ratio of the gas sample fuel-air ratio to the metered fuel-air ratio. In this paper, emission indices based on the metered fuel-air ratios have been used for engine B tests, and emission indices based on the gas sample fuel-air ratios have been used for engine A tests, so that the data presented represent an upper bound on the emission indices with respect to the uncertainty in the fuel-air ratio.

RESULTS AND DISCUSSION

Profile Data

A typical set of temperature and concentration profile data are shown in Figure 2. These data are for test condition 4 (Mach 2.4/19.8 km), engine A. In Figure 2, the horizontal axis on the figures is the radial distance from the engine centerline non-dimensionalized by the calculated nozzle exit radius, R_8, for each test. This radius varies with flight condition and engine power level.

The total temperature distribution across the nozzle diameter for each power level is shown in Figure 2a. At military power (no afterburning), the temperature is quite uniform across the exhaust plane, but for afterburning power significant temperature gradients exist across the diameter. The data shown have been corrected for radiation errors.

The local fuel-air ratios (f/a) calculated from the gas sample measurements are shown in Figure 2b. The corresponding oxides of nitrogen concentration profiles are shown in Figure 2c. From Figures 2a, b, and c, it is evident that the distribution of temperature, local f/a, and NO_x concentration have the same shape. The similarity of the f/a and temperature profiles, and the increase in the average temperature with increasing power level is expected, since increasing the fuel-air ratio increases the temperature for all fuel-air ratios less than stoichiometric. Although the NO_x concentration profiles show a similar shape to the temperature and f/a profiles, the NO_x concentration increases only slightly with increasing power level in afterburning. For all afterburning conditions, the NO_x concentration at mid-radius (downstream of the afterburner flame

holders), was greater than at the same radius at military power. However, the NO_x concentration on the engine centerline was less in afterburning than at military power.

The carbon monoxide and unburned hydrocarbon concentration profiles are shown in Figures 2d, and 2e, respectively. For this flight condition, concentrations of CO and HC for minimum and intermediate afterburning conditions are substantially higher in the center of the exhaust than at the mid to max radial locations. At maximum afterburning, hydrocarbon concentrations in the center have decreased substantially, although a center peak is still evident. Carbon monoxide also still shows a center peak, however, the striking feature of the CO data at maximum afterburning is the appearance of twin regions of high concentration downstream of the afterburner flame holders. Examination of the fuel-air ratio profiles in Figure 2b shows that the local fuel-air ratio is near stoichiometric at these locations, thus the high CO levels represent an approach to equilibrium CO rather than combustion inefficiency. The CO and HC emissions at military power are low (CO < 32 ppmv, HC < 11 ppmC) and uniform across the exhaust. To avoid congestion on the figures, these are not shown.

Although the profile data shown in Figure 2 are typical, significant differences in distribution were observed for different engines, flight speeds, and altitudes. With respect to the NO_x concentration profiles, most conditions exhibit the character shown in Figure 2c. That is, the NO_x concentration downstream of the flame holders for afterburning conditions is greater than at the same radius for military power, but that

near the engine centerline, the NO_x concentration in afterburning is less than at military power. Exceptions to this pattern occurred for afterburning conditions whenever the hydrocarbon concentration and the carbon monoxide concentration in the center region were very low. For these conditions, the NO_x concentration was greater than at the corresponding military power condition at all radii.

In general, the high carbon monoxide and hydrocarbons in the center region decrease both in peak concentration and radial extent with increasing power level, decreasing altitude, or increasing flight speed. The twin peaks in the CO distribution at maximum afterburning may be stronger or weaker than shown in Figure 2d, depending on the relation of the local fuel-air ratio to stoichiometric conditions.

Integrated Average Emissions

The effect of variations in flight speed and altitude on the average emission indices of NO_x, CO, and HC are discussed in the following paragraphs, and shown in Figures 3-5 and 9-14. On these figures, fuel-air ratios less than 0.02 are at military power (no afterburning) whereas fuel-air ratios greater than 0.02 are for afterburning conditions.

Oxides of nitrogen emissions. - The variation of the oxides of nitrogen emission indices (g NO_2/kg fuel) with altitude and fuel-air ratio at Mach 2.0 is shown in Figure 3. At each altitude, the emission indices at minimum afterburning are less than half the value at military power, since the NO_x concentration (ppmv) at minimum afterburning is very nearly equal to the concentration at military power, and the fuel-air ratio at

minimum afterburning is slightly more than double the value at military power. NO_x concentrations increase in going from minimum to maximum afterburning, but since the concentration increase is proportionately less than the increase in fuel-air ratio, the emission indices decrease slightly. (The solid curves shown here and on Figures 4 and 5 result from the NO_x correlation discussed in the next section). Comparisor of the three altitude conditions shows that the NO_x emissions decrease with increasing altitude. This is expected, since the formation of the oxides of nitrogen during combustion is pressure dependent, and the combustor and afterburner pressures decrease with increasing altitude. For all of these conditions, the combustor inlet temperature and afterburner inlet temperature are constant because engine inlet temperature and rotational speed are constant.

The variation of the oxides of nitrogen emission indices with altitude and power level at Mach 2.8 are shown in Figure 4. The effect of fuel-air ratio and altitude are similar to the effects seen in Figure 3, except that the emission indices are higher, because the combustor inlet temperature is higher.

The variation of the NO_x emissions with flight speed and power level at an altitude of 19.8 km is shown in Figure 5. Since the oxides of nitrogen emissions are mainly dependent on the primary combustor conditions, and since increasing flight speed at constant altitude causes both combustor temperature and pressure to rise, the NO_x emissions increase substantially with increasing flight speed. Oxides of nitrogen emission indices for both engines are shown on Figure 5. The data show that the

average NO_x emissions are nearly equal for the two engines at the same flight conditions. Because the NO_x data in [10] (engine A) were not corrected to zero ambient humidity, values given in that reference are from 5 to 15 percent lower than the values shown here.

For the range of flight conditions tested, the average concentration of the oxides of nitrogen at military power (no afterburning), varied from 80 to 170 ppmv, corresponding to emission indices from 8 to 21. The average concentrations of NO_x at minimum afterburning were approximately equal to the concentrations at military power, but increased by about 50 percent from minimum to maximum afterburning. Since the fuel-air ratio in afterburning was from 2 to 4 times that at military power, the NO_x emission indices for afterburning conditions were less than half the emission indices without afterburning.

For any flight condition, the effect of afterburning on the NO_x emission rate (kg/hr) can be determined by examining the variation of the product of the NO_x EI and the f/a with increasing afterburning fuel-air ratio, since engine airflow does not vary with power level. For low afterburning power levels, the NO_x emission rate is nearly equal to its level at military power (no afterburning). The emission rate increases slightly with increasing power in afterburning, at maximum afterburning the NO_x emission rate is approximately 50 percent greater than the value at military power.

Correlation for the oxides of nitrogen emissions. - The effects of combustor parameters on the formation of the oxides of nitrogen from a non-afterburning turbofan engine (TFE 731-2) were correlated in [6] using

the form,

$$NO_x\ EI = C\ \frac{e^{z\theta}\ \delta^{0.5}(f/a)^{1.5}}{(w_a\sqrt{\theta}\ /\delta)} \qquad (1)$$

where θ = combustor inlet total temperature normalized by standard sea level temperature.

δ = combustor inlet total pressure normalized by standard sea level pressure.

f/a = combustor fuel-air ratio, (which is a measure of the exit temperature).

$\frac{w_a\sqrt{\theta}}{\delta}$ = the combustor corrected airflow (which is proportional to the combustor inlet Mach number, M_3, used in [6]).

The results from the J-58 tests at military power can also be successfully correlated with this form as shown in Figure 6. The proportionality constant, C, was determined by a regression analysis using the J-58 data. This correlation shows that effects of combustor inlet temperature, pressure, fuel-air ratio, and combustor inlet Mach number found in reference 6 for a small turbofan engine with a reverse flow combustor, are also appropriate to the J-58, which is a large, axial flow turbojet engine.

For any given engine type, the combustor conditions may be directly related to flight speed, altitude, and power level. For the J-58 data, it was found that the NO_x emissions could be simply correlated with these parameters using the form,

$$NO_x \text{ EI} = 2.53\, e^{M} \left(\frac{P_{amb}}{P_{std}}\right)^{0.3} [1 - 0.57(AB)] \qquad (2)$$

where M = the flight Mach number.

P_{amb} = the static pressure at the flight altitude.

P_{std} = the standard sea level static pressure.

AB = 0 for non-afterburning conditions.

AB = 1 for afterburning conditions.

This correlation is shown in Figure 7. The calculated emission indices agree with the data within ±15 percent. The solid curves in figures 3-5 are the NO_x emission indices calculated with this correlation. The emission index data decrease slightly with increasing afterburning, whereas because of the form chosen for Equation (2), the correlation emission indices are independent of afterburner power level. No doubt the agreement could be improved with a more complicated power level form in Equation (2), but the introduction of the fuel-air ratio as a correlating parameter does not seem justified in view of the satisfactory agreement obtained with the step function. It should be noted that Equation (2) is appropriate for J-58 engines only. Correlation of data from engines of different types must be performed using a form such as given by Equation (1). Of course, the afterburning step function in Equation (2) could also be applied to the correlation form in Equation (1) to extend this form to afterburning conditions.

Comparison of J-58 NO_x emissions with results from other investigations. - Several of the conditions tested at AEDC on the J-93, [5], and J-85, [4],

are within the flight speed-altitude envelope of the J-58 tests (Table 1). The cruise condition for the Concorde (Olympus 593 engine) are also within this envelope. Data for this engine have been reported in [13].

In Figure 8, the variation of the NO_x emission index with Mach number at 19.8 km altitude, and the variation of the NO_x emission index with altitude at Mach 2.0 for the J-58 as given by Equation (2) are shown. Published NO_x emission index data for J-93, J-85, and Olympus 593 engines are also shown. For the J-93 and J-85, the compressor pressure ratios are lower than for the J-58, thus at any given flight condition, the combustor inlet temperatures and pressures are lower, and NO_x emissions are lower. Similarly, the compressor pressure ratio for the Olympus 593 is higher than for the J-58, thus combustor inlet temperatures and pressures are higher, and NO_x emissions are higher for this engine than for the J-58. Although, for any given flight condition, the magnitude of the NO_x emission indices for the J-93, J-85, and Olympus 593 differ from the J-58 NO_x emission index, the variation of the NO_x emission indices with Mach number and altitude for these engines is similar to the variation given by Equation (2) for the J-58.

Carbon monoxide emissions. - The variation of J-58 carbon monoxide emission indices with altitude and power level for Mach 2.0 is shown in Figure 9. For these conditions, the combustor inlet temperature and the afterburner inlet temperature are constant, so the increase in CO emissions with increasing altitude is due to the fact that both the primary combustor and afterburner pressures decrease with increasing altitude, and decreasing pressure causes combustion efficiency to decrease. At each

flight condition, there is a marked increase in CO concentration in going from military power to minimum afterburning. Since the increase in CO concentration is proportionately larger than the increase in fuel-air ratio, the emission indices increase substantially as shown in Figure 9. The further increase in CO emission indices at high fuel-air ratios (maximum afterburning) is due to the high CO concentrations downstream of the flame holders, (see Fig. 2d).

The variation of carbon monoxide emissions with altitude and power level at Mach 2.8 is shown in Figure 10. The trends here are similar to those in Figure 9 for Mach 2.0. The CO emissions increase less rapidly as maximum afterburning is approached at Mach 2.8 than at Mach 2.0 because the overall fuel-air ratio at maximum afterburning for Mach 2.8 is less than for Mach 2.0.

The variation of carbon monoxide emission indices with flight speed and power level at 19.8 km is shown in Figure 11. Results for both J-58 engines are shown, and it is evident that for afterburning modes, the CO emissions from engine A are consistantly higher than for engine B. For both engines, CO emissions decrease with increasing flight speed because combustion efficiency improves with increasing afterburner pressure.

For the range of flight conditions tested, the carbon monoxide emissions at military power were quite low, from 10 to 60 ppmv, which corresponds approximately to emission indices from 1 to 4. Carbon monoxide emission indices at minimum afterburning were approximately an order of magnitude greater than at military power. The CO emissions typically decreased slightly from minimum to intermediate afterburning, but increased

nearly an order of magnitude from intermediate to maximum afterburning.

Unburned hydrocarbon emissions. - The variation of hydrocarbon emission indices with altitude and power level at Mach 2.0 is shown in Figure 12. At military power, the HC concentrations in the exhaust are negligibly small, < 6 ppmC (parts per million carbon by volume), corresponding to emission indices of less than 0.2. The concentrations at minimum afterburning are more than two orders of magnitude greater than at military power. This is a consequence of the region of high unburned hydrocarbons which appears in the center region of the exhaust, see Figure 2e. The peak concentration and radial extent of this region decrease with increasing fuel-air ratio, and the average HC emission indices decrease accordingly. The variation of hydrocarbon emissions with altitude is as expected, with emissions increasing with increasing altitude as afterburner pressure is decreasing.

The variation of hydrocarbon emissions with altitude and power level at Mach 2.8 is shown in Figure 13. At each flight condition, the hydrocarbon emission indices increase substantially from military power to minimum afterburning, then decrease with increasing power in afterburning. The HC concentrations at maximum afterburning are nearly equal to the nonafterburning concentrations. Since the fuel-air ratio at maximum afterburning is about four times that at military power, the HC emission indices at maximum afterburning are about a quarter of the value at military power.

The variation of the hydrocarbon emissions with altitude in afterburning at Mach 2.8 contains a bit of a surprise. Since the afterburner

pressure decreases monotonically from condition 5 to condition 7, the hydrocarbon emissions would be expected to increase monotonically with increasing altitude, as was true at Mach 2.0. However, at Mach 2.8, the highest hydrocarbon emissions occurred at the intermediate altitude conidition. The carbon monoxide and hydrocarbon profiles for these conditions show that both CO and HC profiles have higher concentrations in the center region for condition 6, than for conditions 5 and 7. Since the average hydrocarbon emissions in afterburning are almost exclusively determined by the concentrations in the center (hydrocarbon concentrations at mid to maximum radii are negligible), the effect on the average emissions is very pronounced.

The variation of hydrocarbon emissions with flight speed and power level at 19.8 km is shown in Figure 14. Results for both engines are shown, and it is evident that at the same flight speeds, the hydrocarbon emissions for engine A are substantially higher than for engine B at almost all afterburning power levels.

For the range of flight conditions tested, the hydrocarbon concentrations at military power were almost negligible, < 8 ppmC, which corresponds to emission indices of less than 0.3. At minimum afterburning power levels, the average unburned hydrocarbon emissions were appreciably greater than at military power, but varied over two orders of magnitude as a function of flight speed and altitude. The range of average concentrations was from 10 to 2000 ppmC, which corresponds approximately to emission indices from 0.2 to 20. At all flight conditions, the hydrocarbon emissions decreased with increasing power from minimum to maximum afterburning. For almost

all conditions, the emission indices at maximum afterburning were less than the emission indices at maximum power without afterburning.

Emission levels at the secondary nozzle exit. - The emissions data in this investigation were obtained at the engine primary nozzle where the flow is sonic at a static pressure of from 6 to 15 times the ambient static pressure for each flight altitude. In the aircraft installation, the engine exhaust is expanded through a secondary ejector nozzle and leaves the aircraft at supersonic velocity and at nearly ambient pressure. Chemical kinetics calculations, [14], indicate that the NO_x emission levels should not change appreciably through the secondary nozzle expansion, but that some consumption of CO and HC would be expected in the secondary nozzle flow. Thus, the NO_x emission indices presented in this paper are representative of emissions at the secondary nozzle exit, but the CO and HC emission indices given here represent an upper bound on emissions of these species at the secondary nozzle exhaust.

SUMMARY OF RESULTS

Gaseous emissions from two J-58 afterburning turbojet engines were measured at simulated high-altitude, supersonic flight conditions. For each flight condition, detailed concentration profile measurements were made for four or five engine power levels from military through maximum afterburning. These measurements were made on the horizontal diameter at the engine primary nozzle, using a single point traversing gas sample probe.

The data show that emissions vary with flight speed, altitude, power level, and radial position. The principal results of this investigation

are as follows:

(a) In afterburning modes, there are significant gradients in exhaust temperature, local fuel-air ratio, and species concentration across the exhaust plane. It was found that traverse increments on the order of one tenth of the exhaust radius were required to document these gradients.

(b) Emissions of the oxides of nitrogen (NO_x) decreased with increasing altitude at constant flight speed, and increased with increasing flight speed at constant altitude. The NO_x emission indices at military power (no afterburning), varied from 8 to 21 over the range of altitudes and flight speeds tested. For each flight condition, the NO_x emission indices in afterburning were less than half of the value at military power.

(c) The NO_x emission indices, both with and without afterburning, were correlated with flight speed, altitude, and power level. The NO_x emission indices at military power were correlated in terms of the primary combustor inlet parameters (temperature, pressure, and fuel-air ratio), with a form used previously for data from other engines.

(d) Emissions of carbon monoxide (CO) increased with increasing altitude at constant flight speed, and decreased with increasing flight speed at constant altitude. The CO emission indices at military power varied from 1 to 4 over the range of altitudes and flight speeds tested. CO emission indices for minimum afterburning conditions were approximately an order of magnitude greater than at military power. CO emissions typically decreased slightly from minimum to intermediate afterburning, but increased nearly an order of magnitude from intermediate to maximum afterburning.

(e) Emissions of unburned hydrocarbons (HC) generally increased with increasing altitude at constant flight speed, and decreased with increasing flight speed at constant altitude. The HC emission indices at military power were less than 0.3 for all test conditions. For afterburning conditions, HC emissions were often substantially higher than at military power due to high hydrocarbon concentrations in the center of the exhaust. At minimum afterburning, the HC emission indices varied from 0.2 to 20 for the range of flight speeds and altitudes tested. At all flight conditions, HC emissions decreased with increasing power level in afterburning.

(f) Data for test conditions which were run on both engines showed that the exhaust emissions of CO and HC for the two engines were similar at military power, but quite different for afterburning conditions. The NO_x emissions were very similar for both engines at all power levels.

REFERENCE.

1. Diehl, L. A., "Preliminary Investigation of Gaseous Emissions from Jet Engine Afterburners," NASA Tech Memo X-2323, National Aeronautics and Space Administration, Washington, D.C., July 1971.

2. Palcza, J. L., "Study of Altitude and Mach Number Effects on Exhaust Gas Emissions of an Afterburning Turbofan Engine," NAPTC-ATD-212, Naval Air Propulsion Test Center (AD-741249; FAA-RD-72-31), Trenton, N.J., 1971.

3. Diehl, L. A., "Measurement of Gaseous Emissions from an Afterburning Turbojet Engine at Simulated Altitude Conditions," NASA Tech Memo X-2726, National Aeronautics and Space Administration, Washington, D.C., Mar. 1973.

4. German, R. C., High, M. D., and Robinson, C. E., "Measurement of Exhaust Emissions from a J-85-GE-5B Engine at Simulated High-Altitude Supersonic Free-Stream Flight Conditions," ARO-PWT-TR-73-49, ARO Inc. (AD-764-717; AEDC-TR-73-103; FAA-RD-73-92), Arnold Air Force Station, Tenn., 1973.

5. Davidson, D L., and Domal, A. F., "Emission Measurements of a J-93 Turbojet Engine," ARO-ETF-TR-73-46, ARO Inc. (AD-766648; AEDC-TR-73-132; FAA-RD-73-66), Arnold Air Force Station, Tenn., 1973.

6. Diehl, L. A., and Biaglow, J. A., "Measurement of Gaseous Emissions From a Turbofan Engine at Simulated Altitude Conditions," NASA Tech Memo X-3046, National Aeronautics and Space Administration, Washington, D.C., Apr. 1974.

7. Farlow, N. H., et al., "Measurements of Supersonic Jet Aircraft Wakes in the Stratosphere," Second International Conference on the Environmental Impace of Aerospace Operations in the High Atmosphere, American Meteorology Society, Boston, 1974, pp. 53-58.

8. Holdeman, J. D., "Dispersion and Dilution of Jet Aircraft Exhaust at High Altitude Flight Conditions," Journal of Aircraft, Vol. 11, No. 8, Aug. 1974, pp. 483-487.

9. Holdeman, J. D., "Gaseous Exhaust Emissions From a J-58 Engine at Simulated Supersonic Flight Conditions," NASA Tech Memo X-71532, National Aeronautics and Space Administration, Washington, D.C., Apr. 1974.

10. Holdeman, J. D., "Emission Calibration of a J-58 Afterburning Turbojet Engine at Simulated Supersonic, Stratospheric Flight Conditions," Second International Conference on the Environmental Impact of Aerospace Operations in the High Atmosphere, American Meteorology Society, Boston, 1974, pp. 65-72.

11. "Procedure for the Continuous Sampling and Measurement of Gaseous Emissions From Aircraft Turbine Engines," Aerospace Recommended Practice 1256, SAE, Oct. 1971.

12. Marchionna, N. R., Diehl, L. A., and Trout, A. M., "Effect of Inlet-Air Humidity, Temperature, Pressure, and Reference Mach Number on the Formation of Oxides of Nitrogen in a Gas Turbine Combustor," NASA Tech Note D-7396, National Aeronautics and Space Administration, Washington, D.C., Oct. 1973.

13. Scott, C. J., Olympus 593 Concorde, Emission Characteristics of Representative Current Engines, Ch. 4, CIAP Monograph 2, 1974.

14. Hoshizaki, H., et al., "Study of High-Altitude Aircraft Wake Dynamics. Task 1: Problem Definition," Lockheed Missiles and Space Co. (AD-754918; DOT-TST-90-3), Palo Alto, Calif., 1972.

TABLE 1 - TEST CONDITIONS

Condition	Flight Mach No.	Altitude, km
1	2.0	16.0
2	2.0	17.9
3	2.0	19.8
4	2.4	19.8
5	2.8	19.8
6	2.8	22.0
7	2.8	23.5
8	3.0	19.8

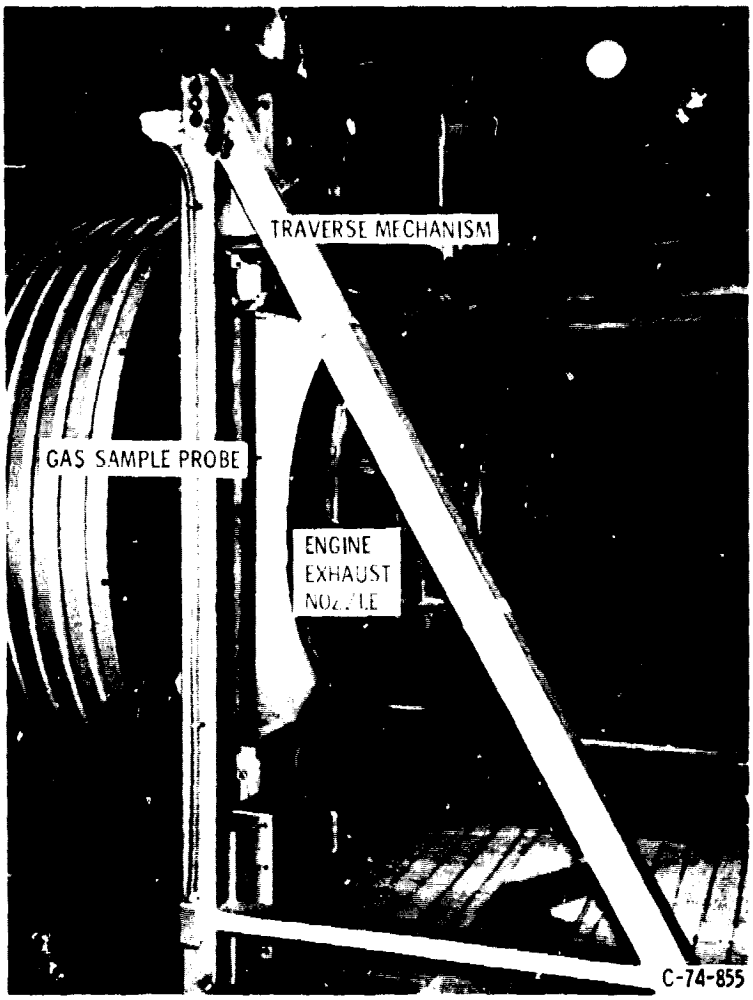

(a) PROBE AND TRAVERSING MECHANISM.

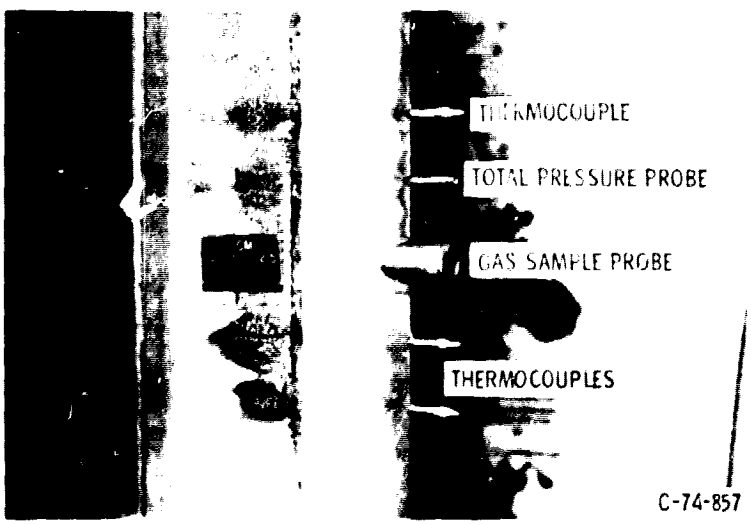

(b) DETAIL OF SENSOR AREA.

Figure 1. - Gas sample probe.

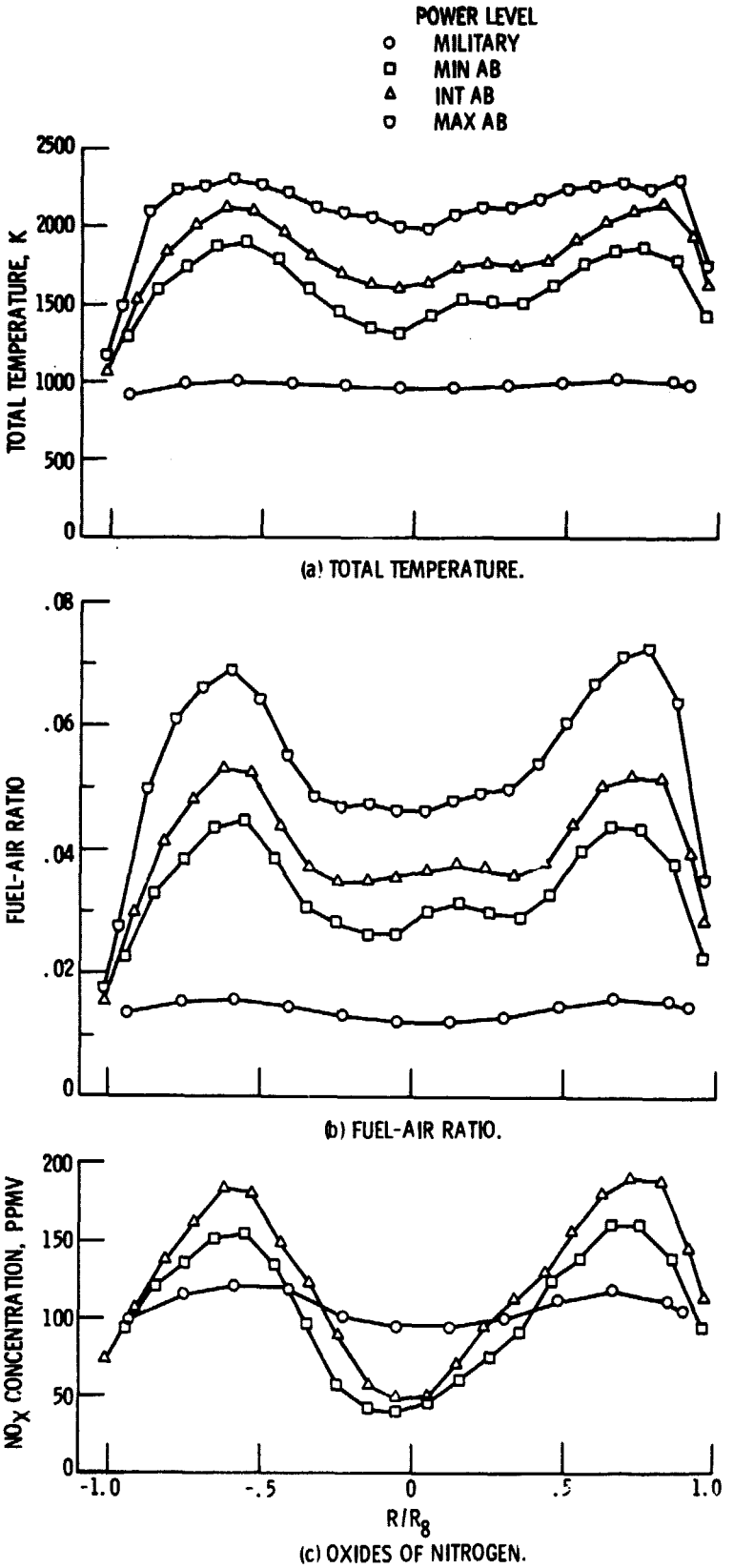

Figure 2. Temperature and concentration profiles for condition A (Mach

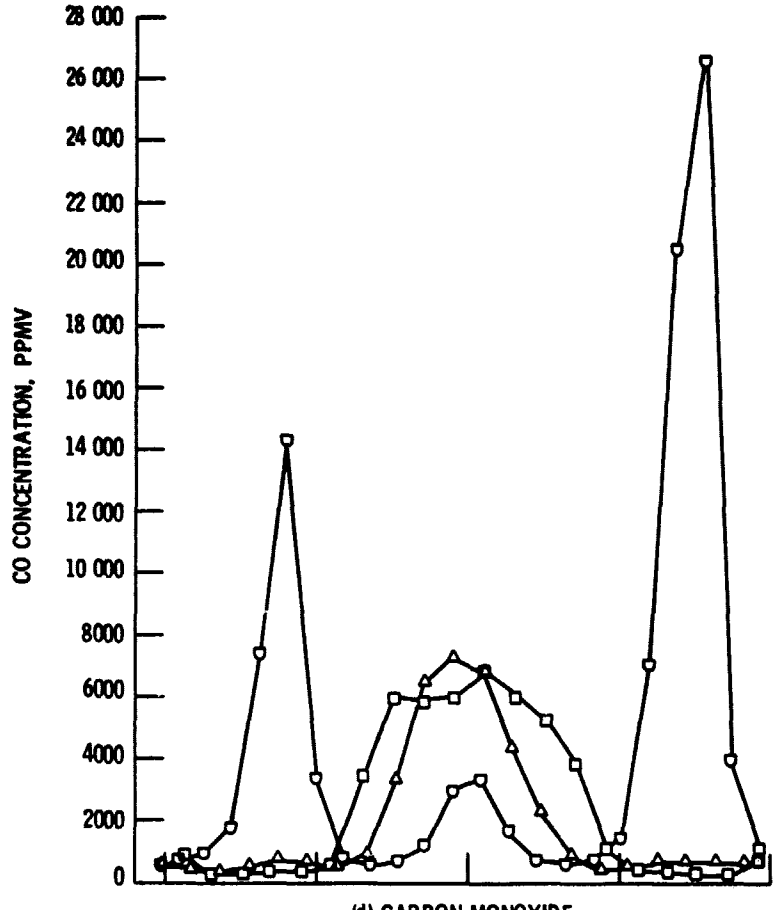

(d) CARBON MONOXIDE.

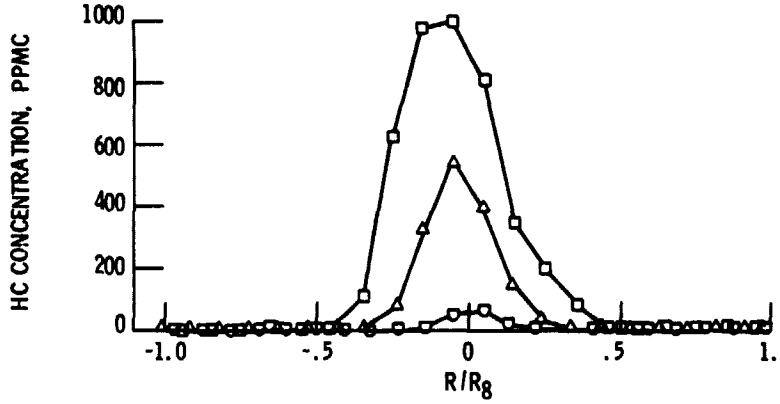

(e) UNBURNED HYDROCARBONS.

Figure 2. - Concluded.

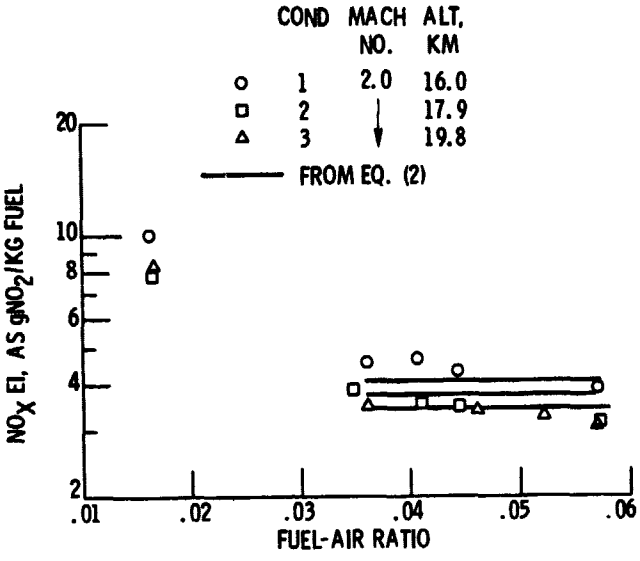

Figure 3. - Variation of oxides of nitrogen emission indices with altitude and power level at Mach 2.0, Engine B.

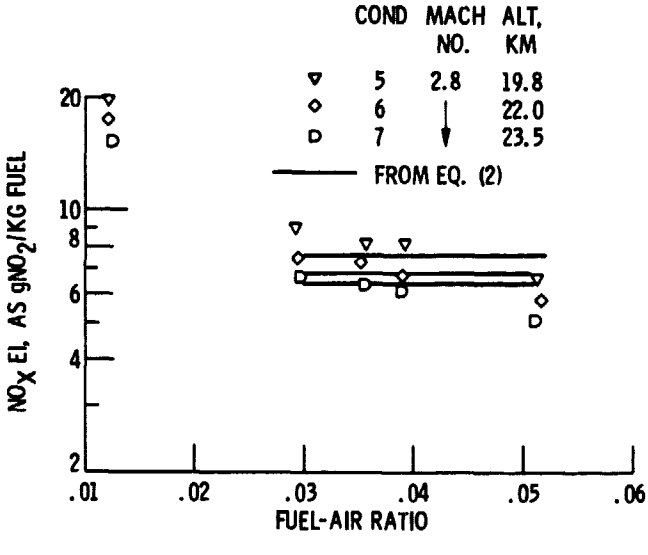

Figure 4. - Variation of oxides of nitrogen emission indices with altitude and power level at Mach 2.8, Engine B.

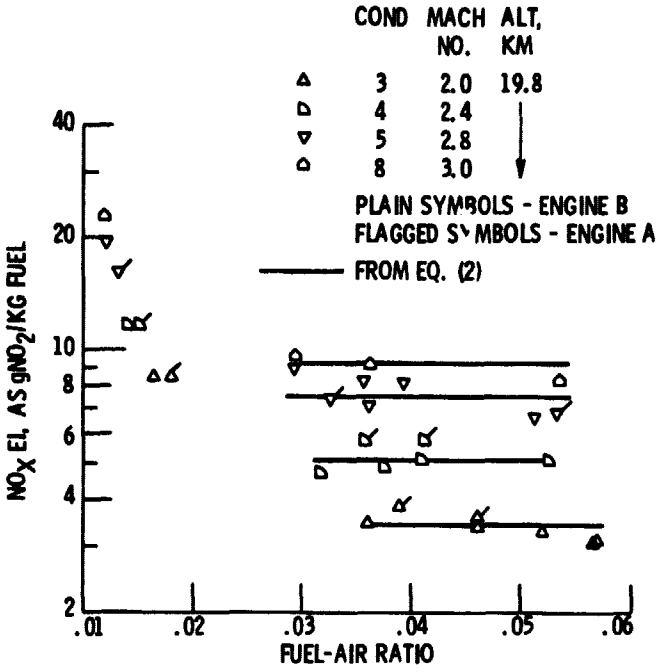

Figure 5. - Variation of oxides of nitrogen emission indices with flight speed and power level at 19.8 kilometers.

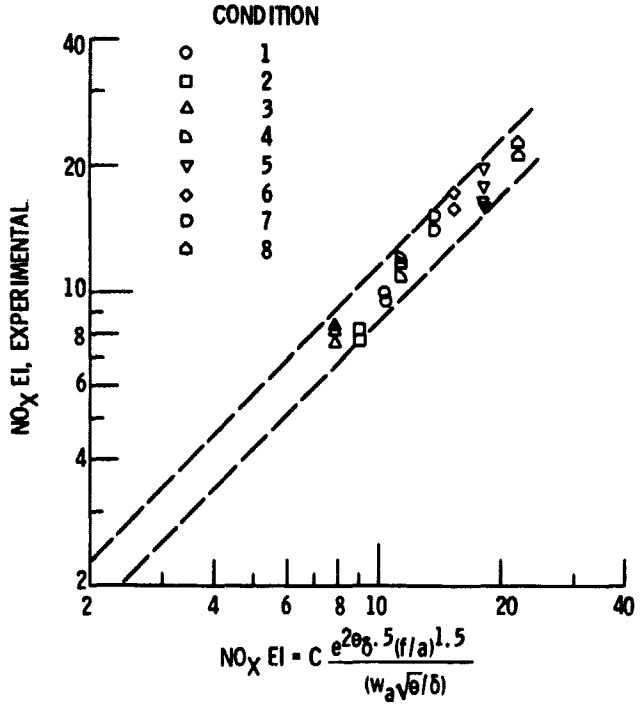

Figure 6. - Correlation of J-58 NO_x emission index with combustor parameters; military power.

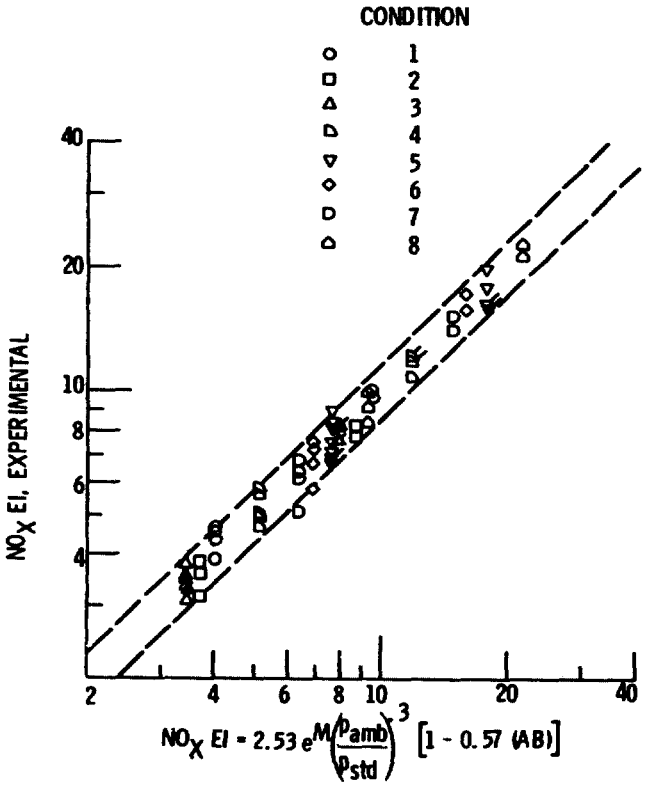

Figure 7. - Correlation of J-58 NO_X emission index with flight parameters; AB = 0 for military power and AB = 1 for afterburning.

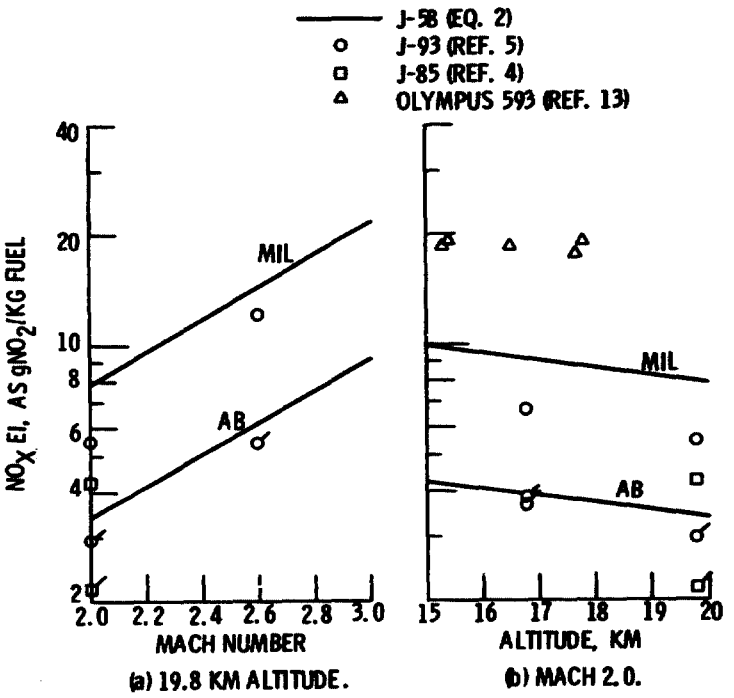

Figure 8. - Comparison of NO_X emission indices for the J-58, J-93, J-85, and Olympus 593. Plain symbols are without afterburning; flagged symbols are with afterburning.

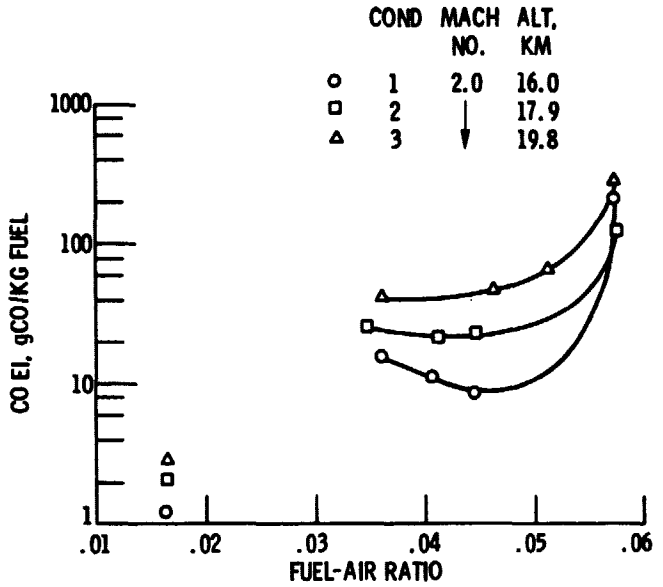

Figure 9. - Variation of carbon monoxide emission indices with altitude and power level at Mach 2.0, Engine B.

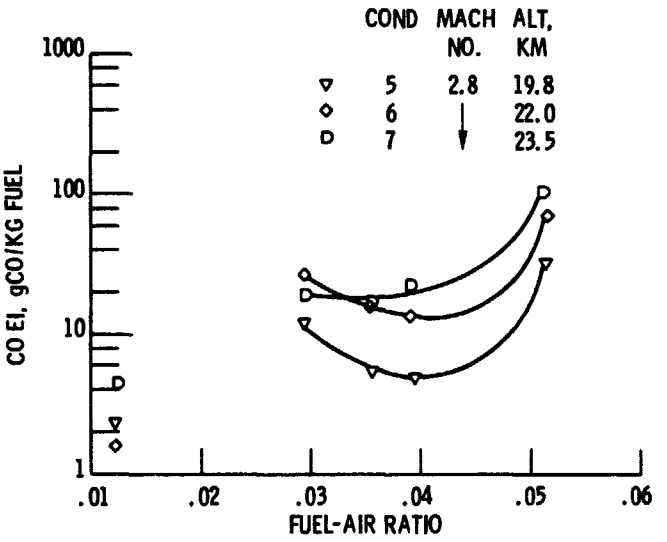

Figure 10. - Variation of carbon monoxide emission indices with altitude and power level at Mach 2.8, Engine B.

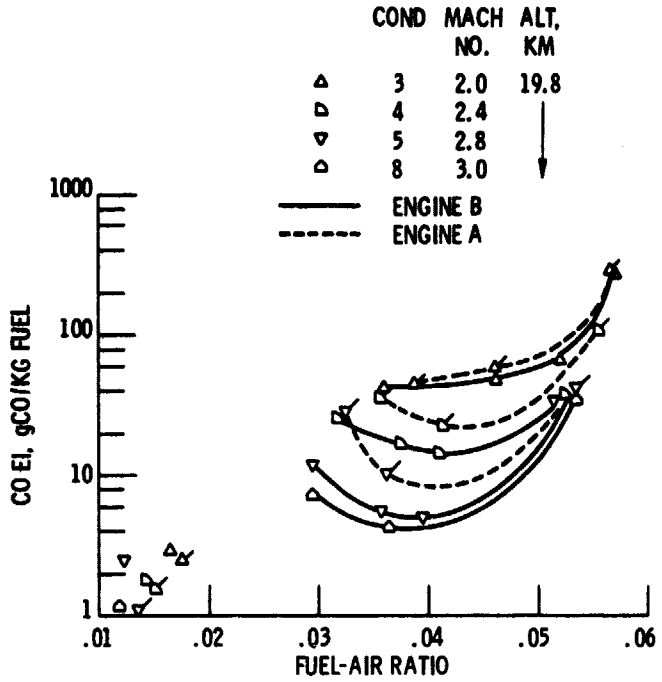

Figure 11. - Variation of carbon monoxide emission indices with flight speed and power level at 19.8 kilometers. Plain symbols are for Engine B, flagged symbols are for Engine A.

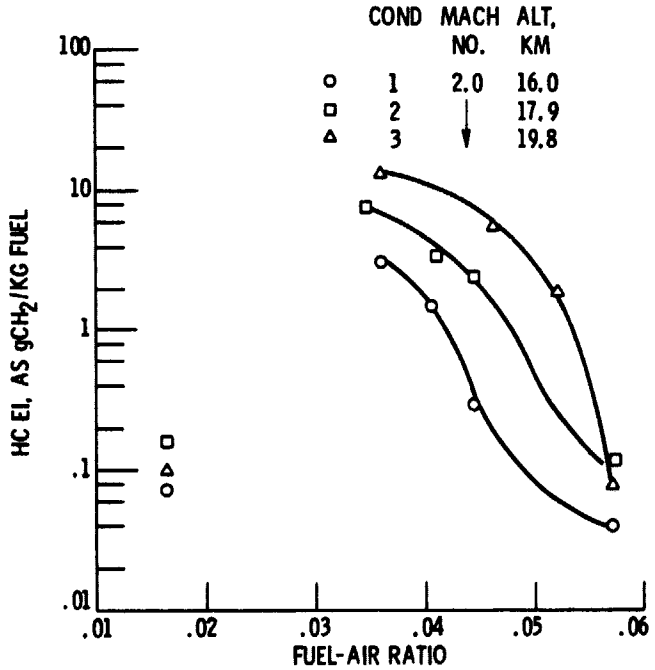

Figure 12. - Variation of hydrocarbon emission indices with altitude and power level at Mach 2.0, Engine B.

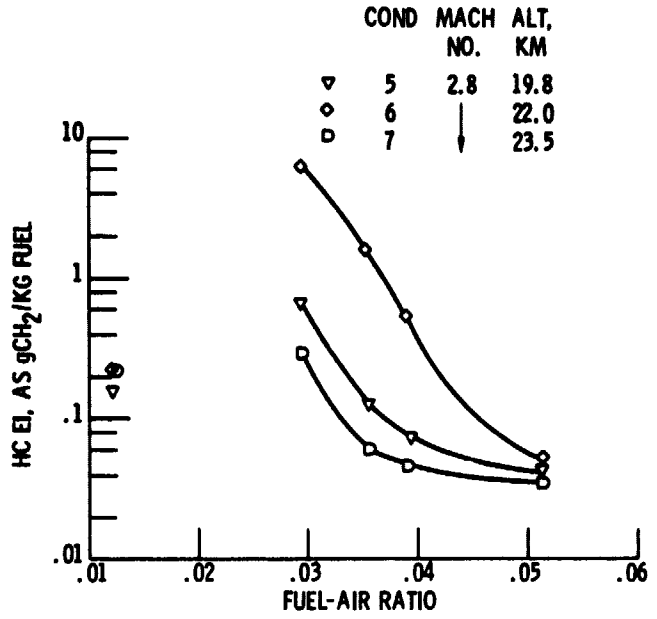

Figure 13. - Variation of hydrocarbon emission indices with altitude and power level at Mach 2.8; Engine B.

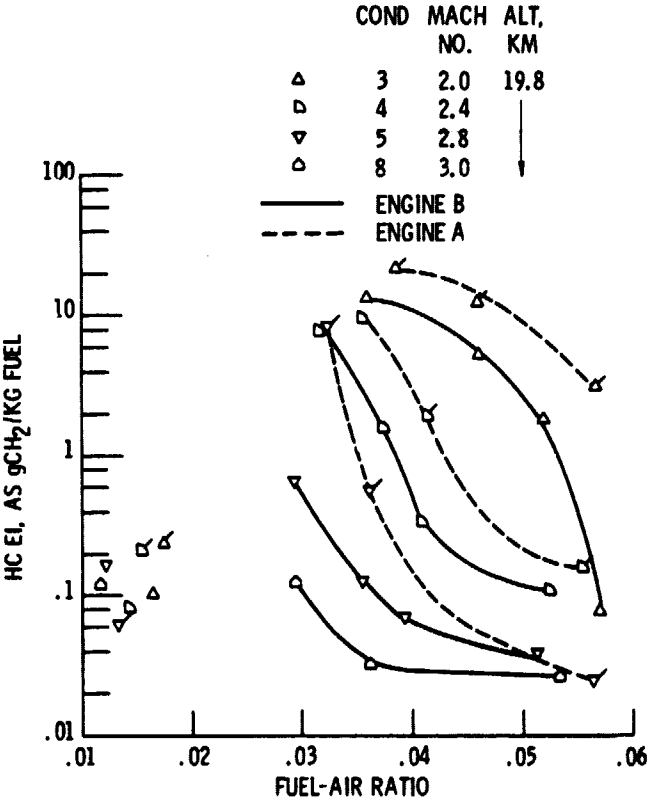

Figure 14. - Variation of hydrocarbon emission indices with flight speed and power level at 19.8 kilometers. Plain symbols are for Engine B, flagged symbols are for Engine A.